RNA
A PUBLICATION OF THE RNA SOCIETY

Metal binding and substrate positioning by evolutionarily invariant U6 sequences in catalytically active protein-free snRNAs

Caroline Lee, Yasaman Jaladat, Afshin Mohammadi, et al.

RNA 2010 16: 2226-2238 originally published online September 8, 2010
Access the most recent version at doi:10.1261/rna.2170910

Metal binding and substrate positioning by evolutionarily invariant U6 sequences in catalytically active protein-free snRNAs

CAROLINE LEE,[1] YASAMAN JALADAT,[1] AFSHIN MOHAMMADI, ARMIN SHARIFI, SARAH GEISLER, and SABA VALADKHAN

Center for RNA Molecular Biology, Case Western Reserve University, Cleveland, Ohio 44106, USA

ABSTRACT

We have previously shown that a base-paired complex formed by two of the spliceosomal RNA components, U6 and U2 small nuclear RNAs (snRNAs), can catalyze a two-step splicing reaction that depended on an evolutionarily invariant region in U6, the ACAGAGA box. Here we further analyze this RNA-catalyzed reaction and show that while the 5′ and 3′ splice site substrates are juxtaposed and positioned near the ACAGAGA sequence in U6, the role of the snRNAs in the reaction is beyond mere juxtaposition of the substrates and likely involves the formation of a sophisticated active site. Interestingly, the snRNA-catalyzed reaction is metal dependent, as is the case with other known splicing RNA enzymes, and terbium(III) cleavage reactions indicate metal binding by the U6/U2 complex within the evolutionarily conserved regions of U6. The above results, combined with the structural similarities between U6 and catalytically critical domains in group II self-splicing introns, suggest that the base-paired complex of U6 and U2 snRNAs is a vestigial ribozyme and a likely descendant of a group II-like self-splicing intron.

Keywords: U6; snRNA; ribozyme; spliceosome; catalysis

INTRODUCTION

Intriguing structural and functional similarities between the spliceosomal snRNAs and group II self-splicing introns, ribozymes which catalyze a splicing reaction mechanistically identical to that performed by the spliceosome, suggest that the snRNAs may have evolved from group II intron-like ancestors (Dayie and Padgett 2008; Toor et al. 2008; Michel et al. 2009; Keating et al. 2010). While formal proof for such an evolutionary relationship is currently lacking, these striking parallels have led to the hypothesis that the snRNAs may also harbor vestigial catalytic activity (Sharp 1985; Cech 1986; Collins and Guthrie 2000; Valadkhan 2007). We have previously shown that in vitro–transcribed, protein-free human U6 and U2 snRNAs can form a base-paired complex that closely resembles the one forming in the spliceosome in its secondary and tertiary structure (Fig. 1A; Valadkhan and Manley 2000; S. Valadkhan and J. Manley, unpubl.). Initial investigations of the catalytic activity of this in vitro–assembled U6/U2 complex indicated that it could catalyze reactions that resembled the first step of splicing in their sequence and ionic requirements, although either the chemistry of the reaction was distinct from splicing or the low efficiency of the reaction prohibited its full characterization (Valadkhan and Manley 2001, 2003; Valadkhan et al. 2007).

More recently, we provided evidence that the same in vitro–assembled U6/U2 snRNA complex was indeed able to perform a two-step splicing reaction on short model substrates (Exon1 and Exon2, Fig. 1B) that led to the formation of a linear RNA product (Fig. 1B; Valadkhan et al. 2009). In the first step of this reaction, an internal phosphodiester bond in the Exon1 substrate is cleaved in a U6/U2-catalyzed hydrolysis reaction. The result is the release of a short "intronic" fragment from the 3′ end of the Exon1 substrate, which now has a free 3′ hydroxyl. The second step of this reaction involves a transesterification between the newly released 3′ OH of Exon1 and an internal phosphate in the Exon2 substrate, which results in the release of an intronic fragment from the 5′ end of Exon2 and ligation of the rest of Exon2 to the Exon1 fragment through a 3′–5′ linkage (Fig. 1B). This two-step splicing reaction is mechanistically identical to the splicing reactions

[1]These authors contributed equally to this paper.

Reprint requests to: Saba Valadkhan, Center for RNA Molecular Biology, Case Western Reserve University, Cleveland, OH 44106, USA; e-mail: sxv46@case.edu; fax: (216) 368-2010.

Article published online ahead of print. Article and publication date are at http://www.rnajournal.org/cgi/doi/10.1261/rna.2170910.

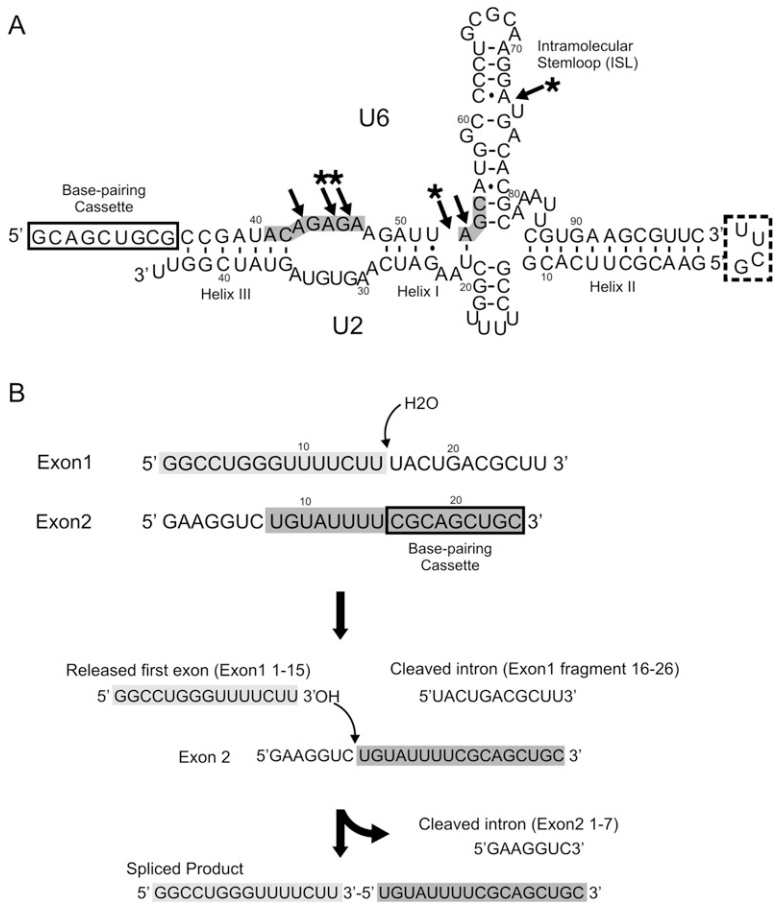

FIGURE 1. The human U6/U2 snRNA complex and the snRNA-mediated splicing reaction. (*A*) The human U6/U2 complex. The location of the base-pairing cassette used for binding Exon2 is shown. Position of helices I, II, and III and the U6 ISL are marked on the complex. Numbers refer to the human numbering system. Arrows point to the previously determined phosphorothioate interference sites. Asterisks mark locations that are also identified as metal binding sites in this study. The boxed nucleotides to the *right* refer to the sequence of a hyperstable loop used to join U6 and U2 together as a single transcript. (*B*) The snRNA-catalyzed splicing reaction. The sequence of Exon1 and Exon2 substrates and the products of each step of the reaction are shown. Numbers refer to position from the 5′ end. "Exonic" sequences are highlighted in gray. The base-pairing cassette in Exon2 used for binding to U6 is shown.

catalyzed by group II introns, the only difference being the use of an internal 2′OH group as the nucleophile of the first step of splicing in these two systems (Moore and Sharp 1993; Nilsen 1998; Lehmann and Schmidt 2003; Pyle and Lambowitz 2006). However, in many group II introns the first step of splicing occurs through hydrolysis, identical to the snRNA-catalyzed reaction described above, which suggests that hydrolysis is a physiological alternative to branching in splicing systems (Chu et al. 1998; Podar et al. 1998).

Interestingly, the snRNA-catalyzed splicing reaction depends on the ACAGAGA and AGC invariant sequences of U6 along with the U6 intramolecular stemloop (ISL) and inner sphere coordination of divalent cations (Valadkhan et al. 2009). Not only are these sequences known to play critical functional roles in spliceosomal catalysis, but sequences analogous to them form the active site of the group II self-splicing introns (Toor et al. 2008; Keating et al. 2010). Further, cross-linking and mutational complementation assays indicated that the reaction indeed occurs in immediate proximity of the evolutionarily invariant ACAGAGA box of U6 (Valadkhan et al. 2009).

The relationship between the catalytic activity of the snRNAs in isolation and their function in the spliceosomal active site, where they are heavily buttressed by proteins, is not clear. The very small size of snRNAs combined with the very large number of spliceosomal proteins make the spliceosome a very unique RNP enzyme and suggest that the structure and function of snRNAs is heavily affected by spliceosomal proteins and thus, comparison of their function in isolation and within the spliceosome will provide fundamental insights into the co-evolution of RNAs and proteins in the spliceosome and other RNP catalytic machines. In order to further investigate the catalytic ability of snRNAs in isolation, we have performed an in-depth characterization of several aspects of the above-described snRNA-catalyzed splicing. Our results indicate that the splice sites on the substrates used in the reaction are positioned in the vicinity of the invariant ACAGAGA sequence of U6 through interactions with this region. We also show that the role of the U6/U2 base-paired complex in catalysis of this two-step splicing reaction is well beyond mere crude juxtaposition of the substrates, suggesting that the U6/U2 complex uses additional catalytic strategies to achieve the observed rate enhancement. We also investigate the cationic requirements of the reaction and show evidence suggesting the involvement of divalent cations in catalysis of this snRNA-mediated splicing reaction. Our structural analysis indicates that similar to what has been observed in vivo and in structural studies, the ISL of U6 is the main metal binding motif in the U6/U2 complex; however, the ACAGAGA and AGC sequences also bind divalent cations. These results provide a first glimpse into the active site of the U6/U2 RNA enzyme and suggest that the invariant, catalytically essential ACAGAGA sequence is not only juxtaposed to and interacts with the substrates, it also binds divalent cations that could help catalyze this metal-dependent reaction.

RESULTS AND DISCUSSION

As a first step toward understanding the catalytic function of the isolated snRNAs, we attempted to gain insight into the organization of the active site. Previous analyses had indicated that at the time of catalysis of the snRNA-mediated reaction, the 5′ splice site equivalent is positioned in the vicinity of the invariant ACAGAGA sequence of U6. Further, we had shown that the substrate carrying the 3′ splice site equivalent (Exon2) interacted with the U6/U2 complex through the sequences at its 3′ end, which formed a functionally required 9-nucleotide (nt)-long base-paired helix with a complementary sequence added to the 5′ end of U6 (Fig. 1; Valadkhan et al. 2009). The addition of this engineered base-pairing cassette was required for enabling the Exon2 substrate to interact with the U6/U2 complex, since unlike the other splicing ribozymes and the spliceosome, the U6/U2 complex does not contain a built-in substrate domain or protein cofactors for assisting with substrate binding. This base-pairing interaction oriented the rest of Exon2, including the 3′ splice site equivalent, toward the ACAGAGA box of U6, which is known to be in immediate proximity of and likely even form part of the spliceosomal active site (Kandels-Lewis and Séraphin 1993; Lesser and Guthrie 1993; Sontheimer and Steitz 1993; Collins and Guthrie 2001; Konarska et al. 2006). In order to gain insight into the positioning of the 3′ splice site equivalent, we first had to determine whether this base-pairing interaction persists throughout the reaction or is disrupted at some point.

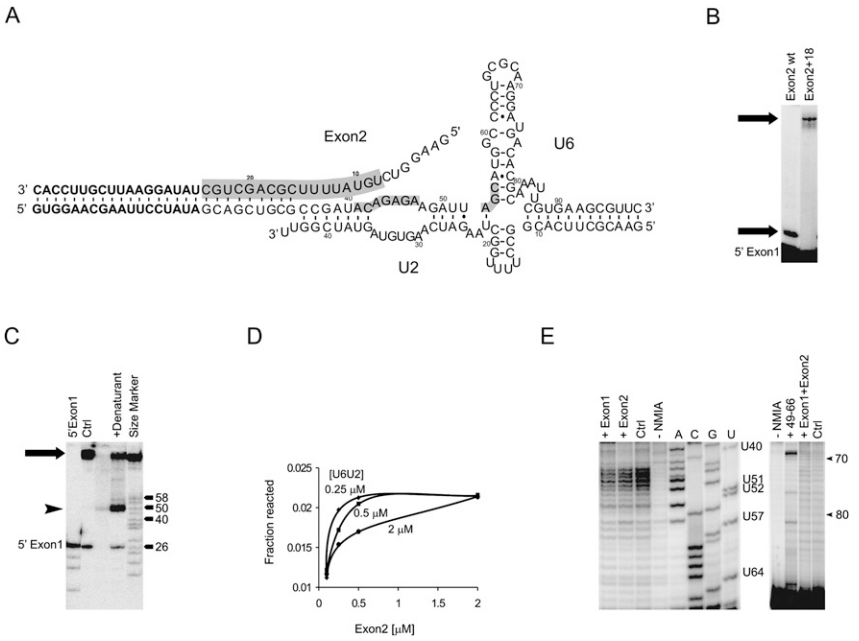

FIGURE 2. Interaction of Exon2 with the U6/U2 complex. (*A*) The U6/U2 complex with elongated base-pairing cassette between Exon2 and U6. The base-pairing interactions between Exon2 and U6 are shown. The sequences added for these experiments are shown in boldface. The "exonic" sequences of the original Exon2 substrate are highlighted in gray. Gray highlights in U6 mark the invariant sequences. (*B*) Exon2 remains associated with the U6/U2 throughout the reaction. Arrows point to the site of products formed with the two different Exon2 species. The location of unreacted Exon1 is shown. (*C*) Denaturation of the product formed with Exon2 + 18, which remains tightly associated with U6 + 18/U2. Lane marked Ctrl contains purified, untreated product. Lane marked +denaturant contains the purified product subjected to strong denaturing treatment. Location of the purified product is shown by an arrow. Arrowhead points to the site of the product released from the U6 + 18/U2 complex after denaturation. The size of several bands in the size marker lane is shown to the *right*. (*D*) Product formation at several U6/U2 and Exon2 concentrations. The Exon2 concentrations are shown at the *x*-axis of the graph. The U6/U2 concentrations are shown next to each set of data in the graph. (*E*) NMIA footprinting analyses on U6 before and after the addition of Exon1 and Exon2 substrates. The *left* panel is probed with a primer binding to the 3′ half of U6 ISL. The *right* panel contains footprinting data obtained with a primer which binds to the helix II region of the U6/U2 complex through U2 (see Materials and Methods). Lanes marked with letters A, C, G, and U are dideoxynucleotide sequencing lanes. Lane marked -NMIA has not received the modification reagent. Lane marked Ctrl contains the results of NMIA modification on U6 in the absence of substrates. Plus (+) sign indicates the ingredients added compared with the Ctrl lane. Lane labeled +49-66 contains an oligonucleotide complementary to U6 nucleotides 49–66. Position of several nucleotides in U6 is shown to the *right*.

To this end, we increased the length of the base-pairing cassette between U6 and Exon2 by 18 nucleotides (Fig. 2A; also see Materials and Methods). We reasoned that a base-paired helix of 27 nucleotides, once formed, will likely remain stably base-paired under the reaction conditions and analysis on nondenaturing gels confirmed that the elongated U6/U2 (U6 + 18/U2) and Exon2 (Exon2 + 18) efficiently associated with each other (data not shown). Catalytic assays performed with Exon2 + 18 and U6 + 18/U2 led to the formation of a very low mobility species, which was identical to the product formed with the original Exon2 and U6/U2 in its formation requirements (Fig. 2B; data not shown). The very low mobility of the product on denaturing PAGE, which moved well above the expected size range, suggested that the formed product was still attached to the U6 + 18/U2 complex. This was confirmed by purifying the low mobility product and denaturing it before reloading it on a denaturing PAGE, which resulted in release of a RNA species of the expected size of 50 nt (Fig. 2C).

The above result proves that the base-pairing interaction between the 5′ end of U6 + 18 and 3′ end of Exon2 + 18 persists during both steps of the reaction. Further, analysis of the extent of product formation at different U6/U2 and Exon2 concentrations indicated that a one-to-one ratio between the original Exon2 and U6/U2 led to optimal

product formation (Fig. 2D), suggesting that even without the 18-nt extension, Exon2 efficiently remained associated with U6/U2 under the reaction conditions. This base-pairing interaction, as mentioned above, orients the rest of Exon2, which includes the 5′ "intronic" domain and the 3′ splice site equivalent, toward the ACAGAGA box of U6. In order to determine if the Exon2 sequences 5′ to the base-pairing cassette interact with the ACAGAGA box, we took a chemical footprinting approach using N-methylisatoic acid (NMIA). NMIA modification monitors the flexibility of nucleotides, and changes in base-pairing or tertiary interactions result in an altered modification pattern (Wilkinson et al. 2006). In the absence of the substrates, NMIA modification on the folded U6/U2 complex led to strong modification at the ACAGAGA sequence, indicating the flexibility of this region (Fig. 2E, left panel). Addition of Exon2 led to a significant protection at this sequence, indicating that the 5′ domain of Exon2 interacts with the ACAGAGA box (Fig. 2E, left panel). As a control, we monitored the modification pattern of U6 ISL with and without the addition of substrates, which did not show any changes (Fig. 2E, right panel), indicating that the altered modification pattern of ACAGAGA was not the result of a global conformational change in the U6/U2 complex. In order to determine whether this was the result of canonical base-pairing or noncanonical interactions between Exon2 and the ACAGAGA box, we performed a DMS modification reaction. The results did not show any alterations in the pattern of DMS modifications, indicating the absence of canonical base-pairing interactions between Exon2 and the ACAGAGA sequence (data not shown).

Taken together, the above results indicate that the base pairing interaction between Exon2 and U6, which is maintained throughout the reaction, orients the 5′ domain of Exon2 toward the ACAGAGA sequence. Modeling the binding of this substrate on the U6/U2 complex suggests that the 3′ splice site equivalent will be positioned next to G44 in the ACAGAGA box (Fig. 2A). Interestingly, cross-linking and mutational complementation analyses indicate that the 5′ splice site equivalent in Exon1 is also positioned in the vicinity of this nucleotide at the time of the reaction, indicating that this sequence of U6 is in immediate vicinity of the site of catalysis in this snRNA-catalyzed reaction.

Exon1 Binds U6/U2 via interactions with the ACAGAGA box

As mentioned above, the first step of the reaction entailed a catalyzed hydrolysis reaction on an internal phosphodiester bond in Exon1 (Fig. 1B). Through cross-linking and mutational complementation studies, we previously showed that nucleotide 14 of Exon1, which was 1 nt upstream of the 5′ splice site equivalent on this substrate, was positioned close to U6 nucleotides G44 and A45 in the ACA**GA**GA box during the reaction (Valadkhan et al. 2009). Unlike Exon2, Exon1 did not seem to have the potential for forming extensive canonical base-pairing interactions with any other RNA in the system and thus, it is likely that its interaction with the U6/U2 complex is mediated via noncanonical interactions (also see Materials and Methods). In order to better understand the positioning of Exon1 in the U6/U2 complex, we took a cross-linking approach to determine whether the rest of Exon1 came in contact with another RNA in the system. We set up typical reactions with an Exon1 species in which the uridine at position 5 of Exon1 was substituted with 4-thio-uridine. UV irradiation of reactions in which either U6 or the 4-thio-uridine substituted Exon1 carried a radioactive label led to the formation of an identical, UV-dependent labeled species (Fig. 3A; data not shown). Radioactive labels on Exon2 or U2 were not incorporated into the cross-link, suggesting that the cross-link was formed between Exon1 and U6 (data not shown). Alkaline hydrolysis reactions on purified cross-linked species carrying a radioactive label at the 5′ end of U6 mapped the cross-link to G54 in the A**G**C triad of U6 (Fig. 3A, right panel).

Modeling Exon1 on U6/U2 indicated that this cross-linked proximity could coexist with the previously described one between residue 14 of Exon1 and the ACAG AGA box of U6/U2 (Fig. 3B). This model places Exon1 in proximity of the U6 ACAGAGA box, helix I, and part of the ISL. We tested the binding of Exon1 to an ISL-like RNA hairpin which contained nucleotides 49–86 of U6 in order to determine whether the ISL played an important role in binding of Exon1, for example, via the interaction of their GC rich sequences, which was not the case (Fig. 3C). To further confirm the above results, we performed NMIA-mediated footprinting (Fig. 2E). While the addition of an oligonucleotide complementary to nucleotides 49–66 of U6 led to a clear change in the pattern of NMIA modifications on U6, the addition of Exon1 and Exon2 substrates did not alter the pattern of modification of the U6 ISL, confirming that their binding was not mediated through interacting with the ISL (Fig. 2E, right panel). However, similar to Exon2, Exon1 caused a significant reduction in the intensity of modification of the ACAGAGA box of U6, indicating that both Exon1 and Exon2 interacted with this critical region of U6 (Fig. 2E, left panel).

To determine the sequences in Exon1 that mediate binding to the U6/U2 complex, we set up reactions in which a trace amount of radiolabeled full-length Exon1 competed with a large excess of unlabeled RNA oligonucleotides for binding to the U6/U2 complex (Fig. 4A). Addition of a 200-fold excess of a random 25-mer RNA oligonucleotide to the reaction did not affect product formation, indicating that it did not detectably disturb the binding and positioning of the substrates or the conformation of the U6/U2 complex or any other aspect of the catalytic activity of the snRNAs (Fig. 4B). The results of addition of RNA oligonucleotides corresponding to different

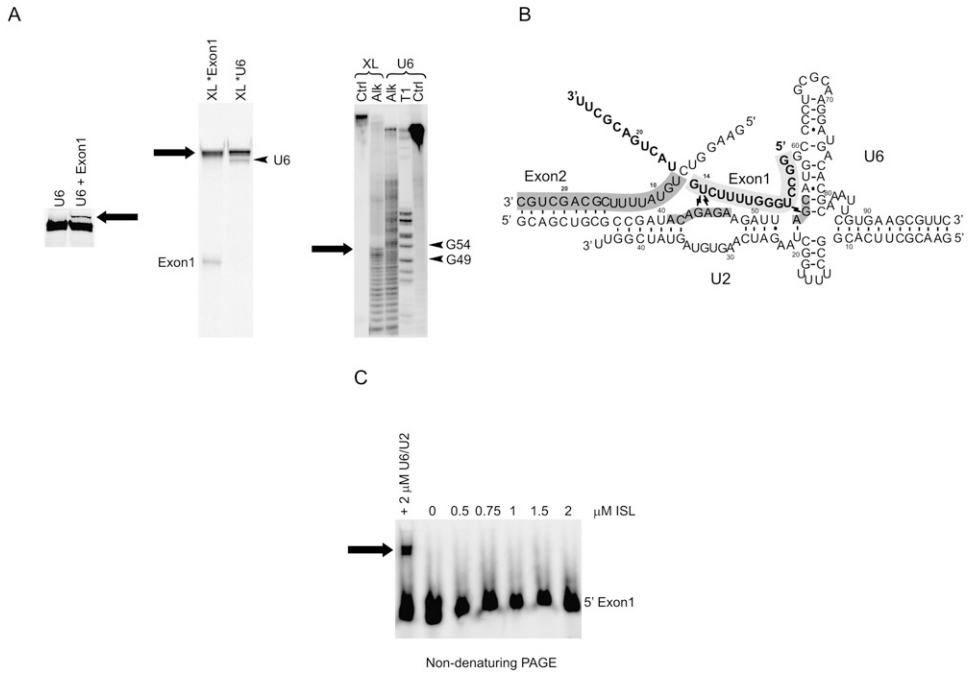

FIGURE 3. Interaction of Exon1 with the U6/U2 complex. (*A*) The uridine at position 5 of Exon1 can be cross-linked to U6 nucleotide 54 in the AGC triad. *Left* panel: the cross-linked band requires Exon1 for its formation. The RNA species present in the cross-linking reaction are indicated on the *top*. Arrow points to the cross-link. Middle panel: an identical cross-linked species forms when Exon1 carries the radiolabel instead of U6. Arrow points to the location of the cross-linked species. Arrowhead marks the site of uncross-linked U6. Location of uncross-linked Exon1 is shown to the *left*. Asterisks indicate the species carrying the radioactive label. *Right* panel: alkaline hydrolysis mapping of the cross-linked nucleotides in U6. Ctrl lanes contain untreated U6 or purified cross-linked species. Lanes marked Alk contain alkaline hydrolysis reactions. An RNase T1 digestion reaction is loaded into the lane marked T1. XL: purified cross-linked species containing a radioactive label at the 5′ end of U6. Arrow points to the site of stop in the hydrolysis ladder. Locations of G49 and 54 in the RNase T1 digestion lane are shown. (*B*) The U6/U2 complex with the bound substrates. The base-pairing interactions between U6 and Exon2 are shown. The highlighted regions in U6 mark the invariant sequences. The highlighted regions in the substrates are the "exonic" sequences. Exon1 is shown in boldface letters. Numbers indicate the human numbering system for U6 and U2 or the position from the 5′ end in the case of the substrates. Thunderbolts mark the nucleotides which can be cross-linked to each other. (*C*) Exon1 does not bind to the U6 ISL in isolation. Location of 5′-labeled Exon1 is shown. The concentration of ISL added to each lane is indicated on *top*. The left-most lane contains the U6/U2 complex instead of ISL. Arrow points to the complex formed between Exon1 and U6/U2.

fragments of Exon1 are summarized in Figure 4A. The addition of RNA oligonucleotides containing nucleotides 1–9 or 1–12 of Exon1, even at 100-fold excess compared with the labeled full-length Exon1, did not block the formation of radiolabeled product although product formation was significantly reduced at the highest concentration of the 1–12 fragment (Fig. 4C). In contrast, oligonucleotides corresponding to nucleotides 1–16 of Exon1 completely eliminated the formation of radiolabeled product (Fig. 4D), indicating that this fragment of Exon1 successfully competed with the labeled full-length Exon1. A fragment containing four additional nucleotides (1–20) blocked the formation of radiolabeled product to the same extent as fragment 1–16, since in both cases a small amount of radiolabeled product could be observed at the lowest concentration of competing oligonucleotides (Fig. 4D). Addition of Exon1 fragments 13–26, 17–26, or 21–26 did not have a dramatic effect on product formation (Fig. 4D,E). These data suggested that residues in the central region of Exon1 mediated its interaction with U6/U2, consistent with the Exon1 protection pattern on U6/U2 and in silico predictions (Fig. 2E; also see Materials and Methods). This conclusion was confirmed by the observation that an Exon1 species in which nucleotides 7–14 were deleted was not able to compete with the labeled full-length Exon1 even when it was at a 100-fold higher concentration compared with the labeled Exon1 (Fig. 4D).

The role of U6/U2 in catalysis is beyond mere juxtaposition of the substrates

The above results and previous data indicate that the two substrates are positioned on U6/U2 in a way that both interact with the invariant ACAGAGA box of U6, and that the 5′ and 3′ splice site equivalents are both in the vicinity of G44 in this sequence at the time of the reaction (Fig. 3B). Previous work also indicated that the observed two-step splicing reaction is a catalyzed reaction and that a number of sequences in U6/U2 are essential for the reaction to occur (Valadkhan et al. 2009). Together, these indicate that

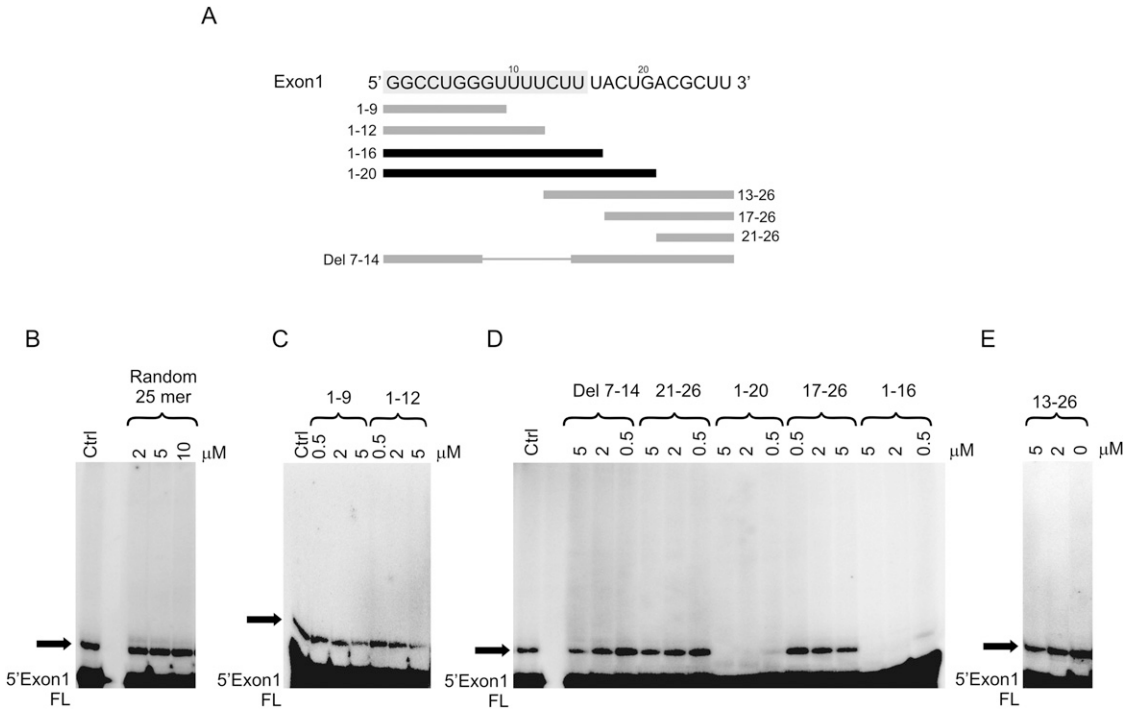

FIGURE 4. Exon1 binds to U6 via its central region. (*A*) The sequence of the full-length Exon1 and the fragments used in competition experiments. The sequence of full-length Exon1 is shown on *top*. Numbers refer to position from the 5′ end. Fragments that could not compete for binding to U6/U2 with Exon1 are shown in light gray, and those that did successfully compete are shown in black. (*B–E*) Exon1 fragments containing the central region of this substrate can block product formation by competing for binding to U6/U2. The identity and concentration of the competing Exon1 fragment or the random RNA oligonucleotide added as a control are shown on *top*. Ctrl: typical reactions that do not contain any competing oligonucleotides. Arrows point to the position of the product. The location of radiolabeled full-length Exon1 (5′ Exon1 FL) is shown to the *left*.

the U6/U2 complex is acting as an enzyme, with the ACAGAGA sequence being in immediate vicinity or forming part of the active site of the reaction. As a first step toward gaining insight into the mode of involvement of U6/U2 in catalysis of this two-step splicing reaction, we asked whether the role of U6/U2 is restricted to mere juxtaposition of the substrates. Since the efficiency of the reaction was low, it was important to determine whether the mere proximity of the two RNA substrates would result in the formation of a product; or if additional, more sophisticated catalytic strategies were employed during the catalysis of the reaction we observed (Narlikar and Herschlag 1997; Fedor and Williamson 2005; Cochrane and Strobel 2008; Wilson and Lilley 2009). We reasoned that if the reaction results from mere juxtaposition of the two substrates, a DNA oligonucleotide should be able to replace the U6/U2 complex as an inert platform by binding to the substrates and orienting them toward each other in a way that recapitulates their spatial orientation in our protein-free splicing reactions.

To this end, we designed two DNA oligonucleotides based on the sequence of U6 snRNA construct used in our experiments and included base-pairing cassettes for Exon2 or both substrates (Fig. 5A). One, U6-5′-60, contained the sequence of U6 construct used in the catalytic reactions from the 5′ end to nucleotide 60, which encompassed all the sequences implicated in interacting with substrates by our analyses including the Exon2 binding cassette (Valadkhan et al. 2009; and see above). The other oligonucleotide, U6-5′-50-α-Ex1, similarly contained the sequence of the U6 construct from the 5′ end to nucleotide 50, which encompassed the Exon2 base-pairing cassette and the ACAGAGA sequence, plus a 9-nt module that was complementary to the first 9 nt of Exon1 and formed an "Exon1 base-pairing cassette" (Fig. 5A). We designed the Exon1 base-pairing cassette in a way that would align nucleotides 5 and 14 of Exon1 in proximity of residues 54 and 44–45 of the U6-like sequence in this oligonucleotide, respectively, in order to mimic the positioning of this substrate in the U6/U2 complex (Valadkhan et al. 2009; also see above).

We set up reactions in which U6/U2 was replaced by one of these two oligonucleotides followed by analysis on denaturing PAGE. To ensure that we could detect even very weak product formation, we used an excess of the radiolabeled Exon1 substrate in these reactions compared with control reactions which contained the original U6/U2 construct (Fig. 5B). We also incubated the reactions for very long time points, or in the presence of several different magnesium concentrations and at different temperatures,

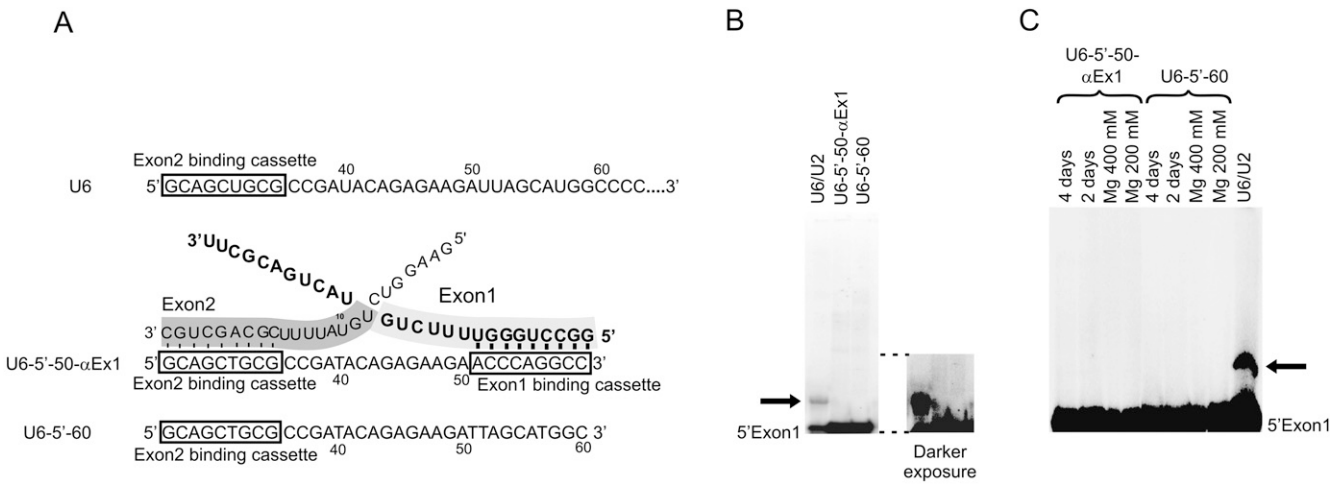

FIGURE 5. The U6/U2 complex plays a role beyond mere juxtaposition of the substrate during the catalysis of the two-step splicing reaction. (*A*) The sequence of the U6-mimic oligonucleotides. The sequence of 5′ end of the U6 construct used in the catalytic assays is shown on *top*. The position of Exon2 binding cassette is indicated. Numbers refer to the human numbering system. The sequence of the two U6-like oligonucleotides is shown below. The Exon2 and Exon1 binding cassettes are shown. The positioning of Exon1 and Exon2 substrates on one of the two oligonucleotides is shown. Exon1 is shown in boldface letters. The gray highlighted regions mark the "exonic" sequences. (*B*) The U6-like oligonucleotides cannot replace the U6/U2 complex in the reaction. The *left* panel contains typical reactions in which U6/U2 is replaced by one or the other U6-like oligonucleotides. A darker exposure of the *bottom* section of the gel is shown in the *right* panel. Lane marked U6/U2 contains a typical reaction. Arrow points to the product. (*C*) The reactions with U6-like oligonucleotides are not rescued at high magnesium concentrations or with long incubations. The identity of the U6-like oligonucleotide added and the reaction condition used is shown on *top*. Lane marked U6/U2 contains a typical reaction. Arrow marks the product. The location of unreacted 5′-labeled Exon1 is shown.

and used both full-length Exon1 and Exon1 1–15 as the substrate to determine if the second step of the reaction in isolation could occur under these conditions (Fig. 5C; data not shown). Analysis of the results of these experiments proved that neither of the reactions containing the oligonucleotides instead of U6/U2 could form any detectable product. This indicated that the role of U6/U2 in catalysis of the two-step splicing reaction is beyond gross juxtaposition of the two substrates and that more sophisticated catalytic strategies, such as general acid/base catalysis using a site-bound metal ion or RNA functional groups, were employed during this reaction. In addition, this result also underscored the significant rate enhancement achieved by the U6/U2 complex in this reaction.

The use of divalent cations in catalysis by U6/U2

Analyses of other ribozymes performing splicing have indicated the extensive use of divalent cations in catalysis (Woodson 2005; Sigel and Pyle 2007). Our previous analyses had indicated that the snRNA-catalyzed splicing reaction did not occur in the presence of even molar concentrations of monovalent cations as the sole cation in the buffer. Replacing magnesium chloride with cobalt hexamine in the buffer, similarly, was not compatible with product formation (Valadkhan et al. 2009), suggesting that inner sphere coordination of a divalent cation may be necessary for the reaction (Roychowdhury-Saha and Burke 2007; Davis et al. 2007). In order to determine if this requirement reflected the use of divalent cations in catalysis during the reaction, we first ensured that magnesium, and not the chloride counterion, is required for the reaction. Analysis of reactions containing magnesium sulfate or magnesium acetate instead of $MgCl_2$ indicated that counterions had at most a minor effect on product formation (Fig. 6A; Heilman-Miller et al. 2001; Woodson 2005). Increasing the concentration of magnesium from 10 to 600 mM in the buffer led to a rise in the extent of product formation (Fig. 6B). In order to determine whether both steps of the reaction or only one step is magnesium dependent, we set up two parallel reactions. Since the first step of the reaction entails catalyzed hydrolysis of an internal phosphodiester bond in Exon1, the products of this step, both of which are smaller than the precursors, have mobilities similar to the degradation products resulting from the long reaction time and high pH and magnesium concentration. Thus, monitoring the first step of the reaction in isolation is not technically feasible. However, by the addition of a shortened Exon1 which only contains the "exonic" sequences and thus resembles the product of the first step of the reaction (Exon1 1–15, Fig. 6C), it is possible to follow the second step of the reaction in isolation (Valadkhan et al. 2009). By comparing the extent of product formation at a gradient of magnesium concentrations in a typical two-step reaction versus the isolated second step, we could demonstrate that the two-step reaction showed a greater enhancement of product formation in response to increased magnesium concentrations (Fig. 6C). This result indicated that both the

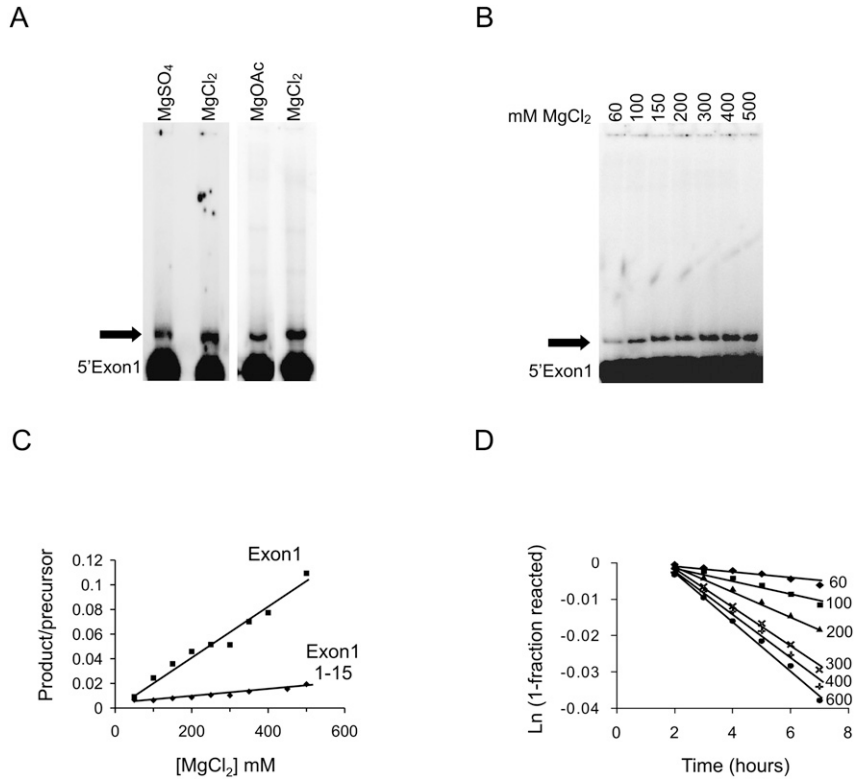

FIGURE 6. Role of metal ions in the snRNA-mediated splicing reaction. Arrows point to the product. Location of unreacted 5′ Exon1 precursor is shown next to each gel panel. (*A*) Use of magnesium acetate or sulfate instead of $MgCl_2$ does not have a significant effect on the reaction. (*B*) The efficiency of product formation is increased as magnesium concentration is raised from 60 to 500 mM. (*C*) The efficiency of product formation in a range of $MgCl_2$ concentrations in a typical two-step splicing reaction versus the isolated second step. The data set labeled "Exon1" is obtained from a typical snRNA-catalyzed two-step splicing reaction. The data set labeled "Exon1 1–15" reflects data from an isolated second step reaction. (*D*) First-order rate constant graphs for reactions performed at $MgCl_2$ concentrations ranging from 60 to 600 mM. The $MgCl_2$ concentration (in mM) for each set of data points is indicated in the graph.

first and the second step of the reaction depended on the presence of divalent cations in buffer.

We performed time course reactions at magnesium concentrations from 60 to 600 mM and determined the rate of the reaction at each concentration (Fig. 6D). These results indicated that the rate of the reaction was increased as the concentration of magnesium was raised in this range. The calculated second-order rate constant was slightly above one, indicating that at least one magnesium ion is involved in the rate-limiting step of the reaction. To determine whether under the reaction conditions catalysis, substrate binding, or another process such as a conformational change was rate limiting, we analyzed the pH dependence of the rate of the reaction. As can be seen from Figure 7A, the reaction is strongly pH dependent and the level of formed product is significantly increased with a rise in pH of the reaction mixture. Analysis of the reaction rate at different pHs followed by calculation of the second-order rate constant showed a linear increase as the pH was changed from 8.0 to 8.8, with a slope of ~1 (Fig. 7B,C). The most likely interpretation of this result is that under the conditions used in these assays, catalysis is the rate-limiting step, with one proton transferred during the step in catalysis which controls the overall rate of the reaction. The above results in aggregate are consistent with a scenario in which catalysis is the rate-limiting step in the snRNA-mediated reactions under the conditions tested, and that the rate of the reaction under these conditions is also magnesium dependent, which can stem from the involvement of divalent cations in a catalytic role in the reaction.

Metal binding by the U6 ISL, ACAGAGA, and AGC sequences

In well-studied ribozymes, site-bound metal ions play critical roles in catalysis and it has been possible to deduce their location using biochemical methods (for example, see Shan et al. 1999; Sigel et al. 2000; Hougland et al. 2005; Forconi et al. 2008; Frederiksen and Piccirilli 2009). As our data are consistent with the involvement of divalent cations in catalysis of the snRNA-mediated splicing, we asked whether we could determine the existence and location of site-specifically bound divalent cations in the U6/U2 complex used in our assays. To this end, we performed terbium(III) cleavage assays (Harris and Walter, 2003; Sigel and Pyle 2003). When present in the reaction mixture at very low concentrations, the sites of cleavage by terbium(III) correspond to site-specific, inner sphere metal binding pockets (Harris and Walter 2003; Sigel and Pyle 2003). In these studies, we used a chimeric U6/U2 complex in which the 3′ end of U6 was joined to the 5′ end of U2 via a UUCG hairpin (Fig. 1A), which ensured that all U6 and U2 molecules were engaged in forming an intermolecular complex. Analysis of the catalytic activity of this construct did not reveal any detectable differences compared with the bimolecular annealed U6/U2 complex (data not shown). Titration of 10–80 μM Tb(III) into the reaction mixture containing the 5′–labeled U6/U2 chimeric construct resulted in the appearance of a number of distinct cleavage sites (Fig. 8). Interestingly, the most intensely cleaved site corresponds to the area in the vicinity of the bulged U (U74) in the U6 ISL (Fig. 8). High-resolution structural studies and phosphorothioate interference analyses in both the spliceosome and group II introns have proved the

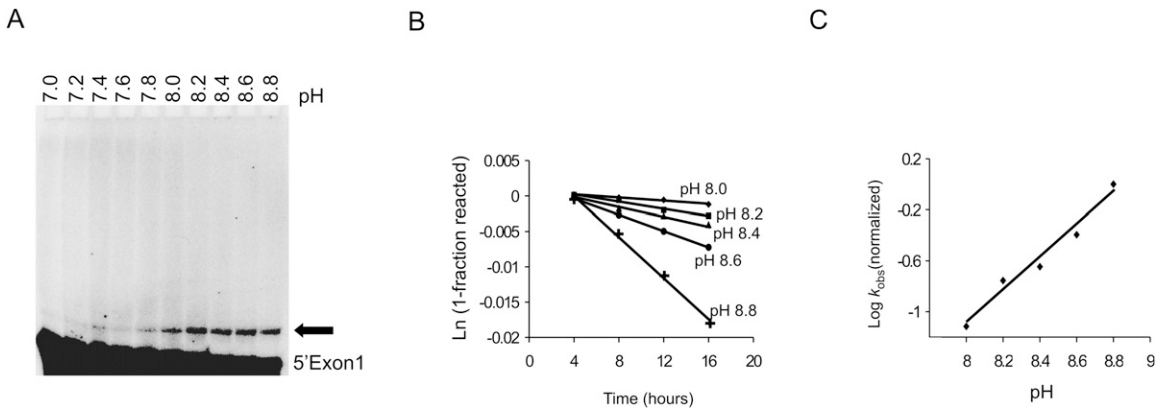

FIGURE 7. The snRNA-catalyzed splicing reaction is pH dependent. (*A*) The efficiency of product formation increases with rising the pH from 7.0 to 8.8. The arrow points to the product. Location of the Exon1 precursor is shown. (*B*) Reaction rate increases as pH is changed from 8.0 to 8.8. (*C*) Second-order rate constant for product formation from pH 8 to 8.8.

presence of a binding pocket for a functionally critical metal ion at this position in the ISL and the equivalent site in Domain V of group II introns (Fig. 1A; Huppler et al. 2002; Valadkhan and Manley 2002; Reiter et al. 2003; Pyle and Lambowitz 2006; Valadkhan 2007; Toor et al. 2008). Thus, this observation proved that our terbium(III) cleavage approach was capable of accurately identifying the site-specific metal binding sites.

Another terbium(III) cleavage site maps to the nucleotides immediately 5′ to the AGC triad of U6, which results from cleavage of the phosphodiester bonds 5′ to nucleotides 52 and 53 (A of AGC) in U6 (Fig. 8). Similar to U74, several lines of data including phosphorothioate interference analyses and biophysical methods implicate the AGC triad of U6 and its analogous AGC sequence in Domain V in coordination of catalytically essential metal ions in the spliceosome and group II introns, respectively (Fig. 1A; Fabrizio and Abelson 1992; Yu et al. 1995; Gordon and Piccirilli 2001; Yuan et al. 2007; Toor et al. 2008). But perhaps most importantly, a third region of cleavage in U6 corresponds to the last nucleotides of the invariant ACAG AGA sequence (Fig. 8). This finding is highly significant, since the ACAGAGA box is known to be in immediate vicinity of the spliceosomal active site and also the active site in the splicing reaction catalyzed by the protein-free U6/U2 in our assays. Further, phosphorothioate interference experiments performed in the authentic spliceosome had indicated that several phosphate oxygens in this region play an important functional role in the spliceosome (Fabrizio and Abelson 1992; Yu et al. 1995). Although a phosphorothioate interference effect by itself does not prove metal binding, two observations make it very likely that the observed interference is due to loss of a critical metal coordination ligand. First, the rescue of a phosphorothioate interference at the 5′ splice site by thiophilic metals proved the direct involvement of divalent cations in catalysis of the first step of splicing (Sontheimer et al. 1997). Second, as mentioned above, some of the sites of phosphorothioate interference at the ACAGAGA sequence are positioned directly adjacent to where the 5′ splice site is positioned at the time of catalysis of the first step (Fabrizio and Abelson 1992; Sontheimer and Steitz 1993; Yu et al. 1995; Konarska et al. 2006). Similarly, in our snRNA-based catalytic system, which is also very likely to use divalent cations during catalysis, the two splice sites are positioned in close proximity of the ACAGAGA sequence and thus, the inner sphere bound metal ions at this region likely correspond to those directly participating in catalysis.

In summary, our analyses of the in vitro catalytic activity of the protein-free U6/U2 complex have indicated several novel aspects of their function. As mentioned above, at the moment our understanding of spliceosomal catalysis is highly rudimentary and whether there is any relationship between the observed catalytic activity of snRNAs in

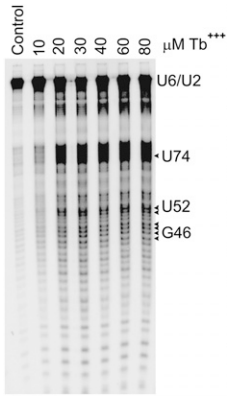

FIGURE 8. Terbium(III) cleavage reactions on folded U6/U2 complexes. Lane marked control does not contain Terbium (Tb+++). The concentration of the added terbium(III) in micromolars is indicated above each lane. The location of unreacted U6/U2 and the position of several residues in U6 is shown to the *right*.

isolation and their function within the spliceosomal active site remains to be proved. However, a number of intriguing parallels which are listed below suggest that the catalytic activity of isolated snRNAs may have a vestigial similarity, at least on the surface, to what we know of the role of snRNAs in the context of the spliceosome. The cross-linking, mutational complementation studies and binding data indicate that in the snRNA-catalyzed reaction, the splice sites are positioned near the ACAGAGA sequence of U6 at the time of the reaction (Valadkhan et al. 2009; this study), similar to what has been previously observed in the spliceosome (Kandels-Lewis and Séraphin 1993; Lesser and Guthrie 1993; Sontheimer and Steitz 1993; Luukkonen and Séraphin 1998; Collins and Guthrie 2001; Konarska et al. 2006). As previously shown, mutations in the ACAGAGA box, the AGC triad and the asymmetric internal loop of U6 ISL have a strong detrimental effect on the reaction in both systems (Fabrizio and Abelson 1990; Madhani et al. 1990; Madhani and Guthrie 1992; Datta and Weiner 1993; Wolff et al. 1994; McPheeters 1996; Hilliker and Staley 2004; Butcher 2009; Valadkhan et al. 2009). Inner sphere coordination of divalent cations is required for the snRNA-catalyzed reaction and kinetic analyses is consistent with the use of divalent cations in catalysis, as has been previously proved in the spliceosome (Sontheimer et al. 1997; Gordon et al. 2000). Further, the metal binding sites in the U6/U2 construct used in the reaction, as determined by terbium(III) cleavage assays, correlate with the sites of phosphorothioate interference observed in the authentic spliceosome and previously determined metal binding sites (Fabrizio and Abelson 1992; Yu et al. 1995; Yean et al. 2000; Huppler et al. 2002; Yuan et al. 2007). While the chemical mechanism of the second step of splicing in the two systems is identical, the first step of splicing in the snRNA-catalyzed reaction proceeds through hydrolysis rather than transesterification. However, the absence of a third substrate in the reaction playing the role of the branch site precludes the possibility of a branching reaction in the protein-free U6/U2 system. Furthermore, hydrolysis represents a physiological alternative to branching as the mechanism of the first step of splicing in group II introns both in vivo and in vitro, and it has been shown that some group II introns which are fully capable of branching use hydrolysis as an alternative mechanism under certain conditions (Chu et al. 1998; Podar et al. 1998).

While the above similarities between the spliceosomal catalysis and the snRNA-mediated splicing reaction are intriguing, determining their significance awaits further studies in both systems. Interestingly, in group II introns the active site is formed by sequences analogous to those playing a critical role in both the spliceosome and the snRNA-mediated reaction (Dayie and Padgett 2008; Toor et al. 2008; Michel et al. 2009; Keating et al. 2010), indicating that these sequences, when correctly positioned, are capable of forming the active site of a splicing machine. While our current knowledge of spliceosomal function cannot rule out the possibility of participation of proteins in splicing catalysis in vivo (Abelson 2008; Newman and Nagai 2010), our work indicates that the snRNAs, once isolated from all other spliceosomal factors, are competent to form a vestigial active site capable of catalyzing splicing. Further analysis of the function of this snRNA complex in parallel with experiments performed in the authentic spliceosome promises to provide fundamental insights into the evolution of RNA enzymes and the way proteins affect the function of RNAs in modern ribozymes and in the long run to uncover any relationship that may exist between the function of snRNAs in isolation and in vivo. Further, with the stepwise addition of spliceosomal proteins to the U6/U2 complex, it may be possible to partially reconstitute the spliceosomal active site for in-depth biochemical and structural biology analyses not currently possible in the authentic spliceosome.

MATERIALS AND METHODS

Preparation of RNA constructs

The wild-type and mutant human U6 and U2 snRNA fragments were prepared by in vitro transcription as described (Valadkhan et al. 2009). The U2 construct used contained nucleotides 1–44 of human U2, with two U to A mutations at nucleotides 2 and 9 and a U to G mutation at nucleotide 41 which helped increase complementarity to U6 in helix II and III regions, respectively. A guanosine residue was added to the 5′ end of U2 to improve transcription efficiency. The U6 construct used contained nucleotides 37–98 of human U6, with a 10-nt extension added to the 5′ end which provided a binding site for Exon2 (see text).

The two substrates, Exon1 and Exon2, were at first designed based on the human 5′ splice site consensus sequence and the branch site consensus sequence, in addition to the domains used for binding to U6/U2 (nucleotides 16–24 of Exon2). The sequence at the 5′ end of Exon1 was selected as a random sequence. The sequence of Exon1 and Exon2 candidates were modified to exclude the constructs which could form stable base-paired structures, both intramolecular and intermolecular (to each other or to ectopic sites on U6/U2). The remaining substrate candidates were tested for binding to each other on nondenaturing gels and those that showed binding were eliminated. The remaining substrate candidates were made by in vitro transcription or chemical synthesis (Dharmacon Biotech, Invitrogen, and Nedken Scientific) at preparative scale. Substrates made by different methods and from different sources showed identical activity in catalytic reactions. Labeling of substrates and U6/U2 at the 5′ end was performed as described (Valadkhan and Manley 2000).

All RNA and DNA constructs were purified from denaturing PAGE at least once, and a small aliquot was labeled at the 5′ end and loaded onto a second denaturing PAGE for quality control. For sequence verification limited RNase T1 digestions were performed. To ensure reproducibility of data, the NTPs and all key reagents were purchased from multiple sources (Sigma, USB, Amresco, and Fisher Scientific).

Catalytic assays

The in vitro–transcribed U6 and U2 snRNA constructs were annealed together in 40 mM Tris, pH 7.2, and 20 mM $MgCl_2$ by heating to 75°C followed by gradual cooling to room temperature in the course of an hour. After annealing, the Exon1 and Exon2 substrates were added at concentrations ranging from 50 nM to 10 μM, depending on the specific reaction. $MgCl_2$ concentration and pH was adjusted to 60 mM and 7.0–8.8, respectively. The final concentration of the U6/U2 complex in a typical reaction was 2 μM. The reaction mixtures were incubated for 6 h at 45°C, for 15 h at 37°C, or for 40 h at 32°C, and product formation was analyzed by running the samples on 12%–20% denaturing PAGE and exposed to PhosphorImager screens.

Analysis of the pH profile of the reaction

Typical catalytic assays were set up as described above at pH ranging from 7.0 to 8.8, and hourly time points were taken. The samples from the final time point of each pH series were loaded side by side to gauge the effect of pH on the final extent of the reaction. The PAGE gels containing the rest of the time course reactions were quantitated using ImageQuant software and the extent of product formation was normalized to the amount of input. The ratio of product formed to precursor in each lane was used to draw an Eadie-Hofstee plot and the second-order rate constant graph, as described (Pyle and Green 1994). The first-order rate constants were normalized to the value of the rate constant at pH 8.8 prior to drawing the second-order rate constant graph.

Analysis of the metal dependence of the reaction

In typical catalytic assays, $MgCl_2$ was replaced by an equal concentration of other salts of magnesium. For determining the effect of different magnesium concentrations on the rate of the reaction, reactions were set up at a gradient of magnesium concentrations and hourly time points were taken. The ionic strength of the reaction was kept constant by the addition of NaCl. Titration of NaCl into the reaction at a constant $MgCl_2$ concentration had an inhibitory effect, indicating that the observed effects cannot be due to an increase in the ionic strength. The rate of the reaction was determined using Eadie-Hofstee plots, as described above.

Terbium(III) cleavage assays

5′-labeled U6/U2 chimeric constructs were folded as described above at a concentration of 50 nM in 10 mM $MgCl_2$ at a pH of 7.2. Next, 10–80 mM $TbCl_3$ was added to the reactions followed by incubation at room temperature for 2–10 h. The reaction mixtures were precipitated and loaded onto a long denaturing PAGE and analyzed after exposing to a PhosphorImager screen.

Exon2 association studies

In order to determine the effect of hyperstabilizing the binding of Exon2 and U6/U2 on the reaction, an 18-nt sequence was added to the 5′ end of U6 (GTGGAACGAATTCCTATA). A complementary sequence was added to the 3′ end of Exon2. Reactions were set up in which the U6 and Exon2 constructs containing these 18 nucleotide extensions replaced the original Exon2 and U6. The resulting low mobility product was purified and denatured for 10 min at 60°C in 10 M urea followed by chilling on ice and loading onto a denaturing PAGE.

Cross-linking analysis

Typical reactions were set up using Exon1 species containing a 4-thio-uridine substitution at position 5 (Dharmacon) and after 2 h of incubation, the reaction mixtures were UV irradiated at 365 nm for 10 min and analyzed on denaturing PAGE. The cross-linked species was gel purified and probed by partial alkaline hydrolysis as previously described (Valadkhan and Manley 2000). Partial RNase T1 digestion reactions on purified product were performed as previously described (Valadkhan and Manley 2000).

Binding assays

A construct containing nucleotides 49–86 of U6, which includes the sequence of the U6 ISL plus two G nucleotides added to the 5′ end and a GUU sequence added to the 3′ end, was made by in vitro transcription and purified from PAGE. Annealing reactions were set up, as described above, in which this construct was added instead of U6 and U2. Labeled Exon1 substrate was added to these reactions along with control reactions which contained the U6/U2 complex. After 2 h of incubation at 30°C, the reactions were loaded onto nondenaturing PAGE and visualized by exposure to PhosphorImager screens.

In silico analysis of Exon1-U6/U2 interactions

We analyzed the sequence of U6 and U2 for potential base-pairing to Exon1 using RNA structure algorithm. Two predicted base-pairing sites containing both canonical and noncanonical base pairs, one between nucleotides 1–6 of Exon1 and nucleotides 55–61 of U6 intramolecular stemloop (ISL), and the other between nucleotides 9–16 of Exon1 and nucleotides 43–50 of U6, were detected. Both could potentially position nucleotide 14 of Exon1 next to the ACAGAGA box. The only other predicted base-pairing interaction was between the 5′ end of Exon1 and the Exon2 binding cassette at the 5′ end of U6, which likely does not contribute to the formation of the product.

NMIA assays

For the NMIA reactions, the preannealed chimeric U6/U2 complex in which the two snRNAs were joined by a hyperstable loop (see above) was used at a concentration of 2 μM in a buffer containing 60 mM magnesium and at a pH of 7.4. The U6/U2 complexes were incubated for 1 h at 30°C with and without the addition of 2 μM Exon1 or Exon2. Freshly prepared solution of NMIA in DMSO was added to the reactions at a final concentration of 0.1 M followed by incubation for 1 h at 30°C (Wilkinson et al. 2006). After the incubation period, the samples were extracted with phenol and chloroform and precipitated.

Following precipitation, the modified RNAs were annealed to an oligonucleotide that was complementary to U6 nucleotides 68–81 or another oligonucleotide that was complementary to U6 nucleotides 93–99, the hyperstable stemloop sequences connecting U6 and U2 and nucleotides 1–45 of U2. The reactions contained 50 mM Tris, pH 8.2, 50 mM KCl, 10 mM $MgCl_2$, 0.5 mM Spermidine, 10 mM DTT, 1 mM of a dNTP mix, and 0.5 U of

AMV reverse transcriptase (Promega) in a total volume of 10 μl and were incubated for 1 h at 40°C. Subsequently the enzyme was heat-inactivated for 2 min at 90°C in 50% formamide and 5 mM EDTA, followed by direct transfer to ice and loading onto a 20% denaturing PAGE.

Exon1 fragment competition studies

The Exon1 fragments were purchased from Nedken Scientific and Invitrogen and were purified from PAGE. Typical reactions were set up which contained 2 μM Exon2, 2 μM U6/U2, and 50 nM 5′-labeled Exon1, and the indicated amount of the Exon1 fragment. The reactions were allowed to proceed for 15 h at 37°C and were loaded onto denaturing PAGE followed by exposing to PhosphorImager screens.

Reactions with U6-like oligonucleotides

The DNA oligonucleotides containing the U6-like sequences were purchased from Invitrogen. Typical reactions were set up which contained 2 μM of one or the other DNA oligonucleotide instead of U6. In some reactions, the magnesium concentration was raised to 200 or 400 mM or the reaction was allowed to proceed for 2 or 4 d instead of the 8-h incubation time used for the control reactions.

ACKNOWLEDGMENTS

We thank Tim Nilsen and Mike Harris for suggestions, insights, and comments on the manuscript. We also thank Aaron Kim, Catherine Tran, Nash Yusuf, Jennifer Biehl, Justin Pruttivarasin, Miriam Israelowitz, and Young-Min Park for technical assistance. This work was supported by a Searle Scholar award from Kinship Foundation, an institutional research grant (IRG–91-022) from the American Cancer Society and NIH grant no. GM078572 to S.V.

Received March 14, 2010; accepted July 31, 2010.

REFERENCES

Abelson J. 2008. Is the spliceosome a ribonucleoprotein enzyme? *Nat Struct Mol Biol* **15:** 1235–1237.

Butcher SE. 2009. The spliceosome as ribozyme hypothesis takes a second step. *Proc Natl Acad Sci* **106:** 12211–12212.

Cech TR. 1986. The generality of self-splicing RNA: Relationship to nuclear mRNA splicing. *Cell* **44:** 207–210.

Chu VT, Liu Q, Podar M, Perlman PS, Pyle AM. 1998. More than one way to splice an RNA: Branching without a bulge and splicing without branching in group II introns. *RNA* **4:** 1186–1202.

Cochrane JC, Strobel SA. 2008. Catalytic strategies of self-cleaving ribozymes. *Acc Chem Res* **41:** 1027–1035.

Collins CA, Guthrie C. 2000. The question remains: Is the spliceosome a ribozyme? *Nat Struct Biol* **7:** 850–854.

Collins CA, Guthrie C. 2001. Genetic interactions between the 5′ and 3′ splice site consensus sequences and U6 snRNA during the second catalytic step of pre-mRNA splicing. *RNA* **7:** 1845–1854.

Datta B, Weiner AM. 1993. The phylogenetically invariant ACAGAGA and AGC sequences of U6 small nuclear RNA are more tolerant of mutation in human cells than in *Saccharomyces cerevisiae*. *Mol Cell Biol* **13:** 5377–5382.

Davis JH, Foster TR, Tonelli M, Butcher SE. 2007. Role of metal ions in the tetraloop-receptor complex as analyzed by NMR. *RNA* **13:** 76–86.

Dayie KT, Padgett RA. 2008. A glimpse into the active site of a group II intron and maybe the spliceosome, too. *RNA* **14:** 1697–1703.

Fabrizio P, Abelson J. 1990. Two domains of yeast U6 small nuclear RNA required for both steps of nuclear precursor messenger RNA splicing. *Science* **250:** 404–409.

Fabrizio P, Abelson J. 1992. Thiophosphates in yeast U6 snRNA specifically affect pre-mRNA splicing in vitro. *Nucleic Acids Res* **20:** 3659–3664.

Fedor MJ, Williamson JR. 2005. The catalytic diversity of RNAs. *Nat Rev Mol Cell Biol* **6:** 399–412.

Forconi M, Lee J, Lee JK, Piccirilli JA, Herschlag D. 2008. Functional identification of ligands for a catalytic metal ion in group I introns. *Biochemistry* **47:** 6883–6894.

Frederiksen JK, Piccirilli JA. 2009. Identification of catalytic metal ion ligands in ribozymes. *Methods* **49:** 148–166.

Gordon PM, Piccirilli JA. 2001. Metal ion coordination by the AGC triad in domain 5 contributes to group II intron catalysis. *Nat Struct Biol* **8:** 893–898.

Gordon PM, Sontheimer EJ, Piccirilli JA. 2000. Metal ion catalysis during the exon-ligation step of nuclear pre-mRNA splicing: Extending the parallels between the spliceosome and group II introns. *RNA* **6:** 199–205.

Harris DA, Walter NG. 2003. Probing RNA structure and metal-binding sites using terbium(III) footprinting. *Curr Protoc Nucleic Acid Chem* **Chapter 6:** Unit 6.8.

Heilman-Miller SL, Pan J, Thirumalai D, Woodson SA. 2001. Role of counterion condensation in folding of the Tetrahymena ribozyme. II. Counterion-dependence of folding kinetics. *J Mol Biol* **309:** 57–68.

Hilliker AK, Staley JP. 2004. Multiple functions for the invariant AGC triad of U6 snRNA. *RNA* **10:** 921–928.

Hougland JL, Kravchuk AV, Herschlag D, Piccirilli JA. 2005. Functional identification of catalytic metal ion binding sites within RNA. *PLoS Biol* **3:** e277. doi: 10.1371/journal.pbio.0030277.

Huppler A, Nikstad LJ, Allmann AM, Brow DA, Butcher SE. 2002. Metal binding and base ionization in the U6 RNA intramolecular stem-loop structure. *Nat Struct Biol* **9:** 431–435.

Kandels-Lewis S, Séraphin B. 1993. Involvement of U6 snRNA in 5′ splice site selection. *Science* **262:** 2035–2039.

Keating KS, Toor N, Perlman PS, Pyle AM. 2010. A structural analysis of the group II intron active site and implications for the spliceosome. *RNA* **16:** 1–9.

Konarska MM, Vilardell J, Query CC. 2006. Repositioning of the reaction intermediate within the catalytic center of the spliceosome. *Mol Cell* **21:** 543–553.

Lehmann K, Schmidt U. 2003. Group II introns: Structure and catalytic versatility of large natural ribozymes. *Crit Rev Biochem Mol Biol* **38:** 249–303.

Lesser CF, Guthrie C. 1993. Mutations in U6 snRNA that alter splice site specificity: Implications for the active site. *Science* **262:** 1982–1988.

Luukkonen BG, Séraphin B. 1998. Genetic interaction between U6 snRNA and the first intron nucleotide in Saccharomyces cerevisiae. *RNA* **4:** 167–180.

Madhani HD, Guthrie C. 1992. A novel base-pairing interaction between U2 and U6 snRNAs suggests a mechanism for the catalytic activation of the spliceosome. *Cell* **71:** 803–817.

Madhani HD, Bordonné R, Guthrie C. 1990. Multiple roles for U6 snRNA in the splicing pathway. *Genes Dev* **4:** 2264–2277.

McPheeters DS. 1996. Interactions of the yeast U6 RNA with the pre-mRNA branch site. *RNA* **2:** 1110–1123.

Michel F, Costa M, Westhof E. 2009. The ribozyme core of group II introns: A structure in want of partners. *Trends Biochem Sci* **34:** 189–199.

Moore MJ, Sharp PA. 1993. Evidence for two active sites in the spliceosome provided by stereochemistry of pre-mRNA splicing. *Nature* **365:** 364–368.

Narlikar GJ, Herschlag D. 1997. Mechanistic aspects of enzymatic catalysis: Lessons from comparison of RNA and protein enzymes. *Annu Rev Biochem* **66:** 19–59.

Newman AJ, Nagai K. 2010. Structural studies of the spliceosome: Blind men and an elephant. *Curr Opin Struct Biol* **20:** 82–89.

Nilsen TW. 1998. RNA-RNA interactions in nuclear pre-mRNA splicing. In *RNA structure and function* (eds. RW Simons and M Grunberg-Manago), pp. 279–307. Cold Spring Harbor Laboratory Press, Cold Spring Harbor, NY.

Podar M, Chu VT, Pyle AM, Perlman PS. 1998. Group II intron splicing in vivo by first-step hydrolysis. *Nature* **391:** 915–918.

Pyle AM, Green JB. 1994. Building a kinetic framework for group II intron ribozyme activity: Quantitation of interdomain binding and reaction rate. *Biochemistry* **33:** 2716–2725.

Pyle AM, Lambowitz AM. 2006. Group II introns: Ribozymes that splice RNA and invade DNA. In *The RNA world* (eds. RF Gesteland, TR Cech, and JF Atkins), pp. 469–506. Cold Spring Harbor Laboratory Press, Cold Spring Harbor, NY.

Reiter NJ, Nikstad LJ, Allmann AM, Johnson RJ, Butcher SE. 2003. Structure of the U6 RNA intramolecular stem-loop harboring an S(P)-phosphorothioate modification. *RNA* **9:** 533–542.

Roychowdhury-Saha M, Burke DH. 2007. Distinct reaction pathway promoted by non-divalent-metal cations in a tertiary stabilized hammerhead ribozyme. *RNA* **13:** 841–848.

Shan SO, Yoshida A, Sun S, Piccirilli JA, Herschlag D. 1999. Three metal ions at the active site of the Tetrahymena group I ribozyme. *Proc Natl Acad Sci* **96:** 12299–12304.

Sharp PA. 1985. On the origin of RNA splicing and introns. *Cell* **42:** 397–400.

Sigel RKO, Pyle AM. 2003. Lanthanide ions as probes for metal ions in the structure and catalytic mechanism of ribozymes. *Met Ions Biol Syst* **40:** 477–512.

Sigel RKO, Pyle AM. 2007. Alternative roles for metal ions in enzyme catalysis and the implications for ribozyme chemistry. *Chem Rev* **107:** 97–113.

Sigel RK, Vaidya A, Pyle AM. 2000. Metal ion binding sites in a group II intron core. *Nat Struct Biol* **7:** 1111–1116.

Sontheimer EJ, Steitz JA. 1993. The U5 and U6 small nuclear RNAs as active site components of the spliceosome. *Science* **262:** 1989–1996.

Sontheimer EJ, Sun S, Piccirilli JA. 1997. Metal ion catalysis during splicing of premessenger RNA. *Nature* **388:** 801–805.

Toor N, Keating KS, Taylor SD, Pyle AM. 2008. Crystal structure of a self-spliced group II intron. *Science* **320:** 77–82.

Valadkhan S. 2007. The spliceosome: A ribozyme at heart? *Biol Chem* **388:** 693–697.

Valadkhan S, Manley JL. 2000. A tertiary interaction detected in a human U2-U6 snRNA complex assembled in vitro resembles a genetically proven interaction in yeast. *RNA* **6:** 206–219.

Valadkhan S, Manley JL. 2001. Splicing-related catalysis by protein-free snRNAs. *Nature* **413:** 701–707.

Valadkhan S, Manley JL. 2002. Intrinsic metal binding by a spliceosomal RNA. *Nat Struct Biol* **9:** 498–499.

Valadkhan S, Manley JL. 2003. Characterization of the catalytic activity of U2 and U6 snRNAs. *RNA* **9:** 892–904.

Valadkhan S, Mohammadi A, Wachtel C, Manley JL. 2007. Protein-free spliceosomal snRNAs catalyze a reaction that resembles the first step of splicing. *RNA* **13:** 2300–2311.

Valadkhan S, Mohammadi A, Jaladat Y, Geisler S. 2009. Protein-free small nuclear RNAs catalyze a two-step splicing reaction. *Proc Natl Acad Sci* **106:** 11901–11906.

Wilkinson KA, Merino EJ, Weeks KM. 2006. Selective 2′-hydroxyl acylation analyzed by primer extension (SHAPE): Quantitative RNA structure analysis at single nucleotide resolution. *Nat Protoc* **1:** 1610–1616.

Wilson TJ, Lilley DMJ. 2009. Biochemistry. The evolution of ribozyme chemistry. *Science* **323:** 1436–1438.

Wolff T, Menssen R, Hammel J, Bindereif A. 1994. Splicing function of mammalian U6 small nuclear RNA: Conserved positions in central domain and helix I are essential during the first and second step of pre-mRNA splicing. *Proc Natl Acad Sci* **91:** 903–907.

Woodson SA. 2005. Metal ions and RNA folding: A highly charged topic with a dynamic future. *Curr Opin Chem Biol* **9:** 104–109.

Yean SL, Wuenschell G, Termini J, Lin RJ. 2000. Metal-ion coordination by U6 small nuclear RNA contributes to catalysis in the spliceosome. *Nature* **408:** 881–884.

Yu YT, Maroney PA, Darzynkiwicz E, Nilsen TW. 1995. U6 snRNA function in nuclear pre-mRNA splicing: A phosphorothioate interference analysis of the U6 phosphate backbone. *RNA* **1:** 46–54.

Yuan F, Griffin L, Phelps L, Buschmann V, Weston K, Greenbaum NL. 2007. Use of a novel Förster resonance energy transfer method to identify locations of site-bound metal ions in the U2-U6 snRNA complex. *Nucleic Acids Res* **35:** 2833–2845.